Ice–Seawater Turbulent Boundary Layer Interaction with Melting or Freezing

GEORGE L. MELLOR

Geophysical Fluid Dynamics Program, Princeton University, Princeton, NJ 08540

MILES G. MCPHEE

McPhee Research Co., Yakima, WA 98908

MICHAEL STEELE

Geophysical Fluid Dynamics Program, Princeton University, Princeton, NJ 08540

(Manuscript received 15 October 1985, in final form 14 April 1986)

ABSTRACT

A second-moment, turbulence closure model is applied to the problem of the dynamic and thermodynamic interaction of sea ice and the ocean surface mixed layer. In the case of ice moving over a warm, ocean surface layer, melting is intrinsically a transient process; that is, melting is rapid when warm surface water initially contacts the ice. Then the process slows when surface water is insulated from deeper water due to the stabilizing effect of the melt water, and the thermal energy stored in the surface layer is depleted. Effectively, the same process prevails when ocean surface water flows under stationary ice in which case, after an initial rapid increase, the melting process decreases with downstream distance. Accompanying the stabilizing effect of the melt water is a reduction in the ice–seawater interfacial shear stress. This process and model simulations are used to explain field observations wherein ice near the marginal ice zone diverges from the main pack.

When the surface ice layer is made to grow by imposing heat conduction through the ice, the surface ocean layer is destabilized by brine rejection and mixing in the water column is enhanced. The heat flux into the water column is a small percentage of the heat conduction through the ice.

1. Introduction

In model simulations of the dynamics and thermodynamics of sea ice, interaction with the ocean has virtually been ignored (Hibler, 1979) although, in the important marginal ice zones, heat transfer from the ocean is an important process in determining the location and physical characteristics of these zones. Recently, Hibler and Bryan (1984) coupled an ice model with an ocean model; no attempt was made to resolve or model the ocean surface layer, the region of direct interaction between the ice and ocean, but they did cite the need for more realistic boundary layer formulations.

A simple dynamic and thermodynamic model of the ocean surface layer under a melting ice pack has been provided by McPhee (1981, 1982, 1983). He recognized the role of density stratification and incorporated known properties of turbulent boundary layers as they are understood from laboratory data. The main deficiency was that the model was a steady state model, which probably provides good estimates of the solutions of the Coriolis-dominated momentum equations but which has difficulty estimating the thermodynamics. In this paper we will show that, in the case of melting ice overlaying warm water, the thermodynamic process is inherently a transient process.

Josberger (1983) also provided a thermodynamic model of the melting ice problem wherein the eddy heat diffusivity was parametrically related to wind stress. Aside from the fact that the model was also a steady state model, his assumed temperature distribution was not realistic, and through analytical error (in computing an Obukhoff length) he concluded that density stratification was not important.

In this paper we introduce a model that is first constrained to horizontally homogeneous fields but which is unsteady. The solutions are then shown to approximate steady flows that are inhomogeneous in one space coordinate. Solutions are obtained numerically and depict the evolution of temperature, salinity and velocity fields and the evolution of surface stress and melt rate. We use a second-moment turbulence closure model to provide mixing coefficients that respond to vertical, velocity and density gradients.

Close attention is given to the interfacial ice–sea boundary conditions wherein it is necessary to combine conventional turbulent boundary layer methodology, involving the law of the wall and roughness parameters, with the proper energy and salinity balances associated

with ice melting or freezing in response to the atmospheric or oceanic environment.

2. The governing equations

We first consider the problem where all properties are horizontally homogeneous. The equations for velocity (U, V), temperature, T, and salinity, S, are

$$\frac{\partial}{\partial t}(U, V) + f(-V, U) = \frac{\partial}{\partial z}\left[K_M \frac{\partial}{\partial z}(U, V)\right] \quad \text{(1a, b)}$$

$$\frac{\partial T}{\partial t} = \frac{\partial}{\partial z}\left[(K_H + \alpha_t)\frac{\partial T}{\partial z}\right] \quad (2)$$

$$\frac{\partial S}{\partial t} = \frac{\partial}{\partial z}\left[(K_H + \alpha_S)\frac{\partial S}{\partial z}\right] \quad (3)$$

where t is time and z the vertical coordinate; $z = 0$ will be positioned at the ice–seawater interface and water will occupy negative z-space. Here f is the Coriolis parameter, and K_M and K_H are the turbulent mixing coefficients for momentum and any scalar variable, about which more will be said later. Although we plan to solve (1a, b), (2) and (3) for large enough negative z so that $K_H \gg \alpha_t$ and $K_H \gg \alpha_S$, we nevertheless include the molecular diffusivities, α_t and α_S, in (2) and (3) as a reminder that continuity with the interfacial flux must ultimately involve molecular diffusion.

We let the boundary conditions for large negative z be

$$(U, V) \sim 0, \quad z \to -\infty \quad \text{(4a, b)}$$

$$T \sim T_\infty, \quad z \to -\infty \quad (5)$$

$$S \sim S_\infty, \quad z \to -\infty. \quad (6)$$

Note that (1a, b) and (4a, b) can be easily modified to include a deep-water geostrophic velocity.

Near the interfacial surface, law-of-the-wall behavior is assumed such that,

$$(U_0 - U, V_0 - V) = -\frac{(\tau_x^0, \tau_y^0)}{k u_\tau} \ln \frac{-z}{z_0}, \quad -z \to z_0 \quad \text{(7a, b)}$$

$$T_0 - T = -\frac{F_t}{k u_\tau} \ln \frac{-z}{z_{0t}}, \quad -z \to z_0 \quad (8)$$

$$S_0 - S = -\frac{F_s}{k u_\tau} \ln \frac{-z}{z_{0s}}, \quad -z \to z_0 \quad (9)$$

where (U_0, V_0), T_0 and S_0 are properties at $z = 0-$, (τ_x^0, τ_y^0) is the kinematic surface-stress (dynamic stress divided by density) vector, $u_\tau^2 \equiv [\tau_x^2 + \tau_y^2]^{1/2}$, and F_t and F_s are the surface heat and salinity fluxes. The application of (7a, b), (8) and (9) as $-z \to z_0$ is a mathematical formalism since the profiles given by these equations are only valid when $-z \gg z_0$. Note that our ignorance of the very-near-surface flow processes is subsumed in the empirical roughness parameters, z_0, z_{0t} and z_{0s}. It will be shown, however, that $z_{0t} \ll z_0$ and $z_{0s} \ll z_0$.

In appendix A, it is shown that (7a, b), (8) and (9) are valid asymptotically for small $|W_0/u_\tau|$ where W_0 is melting (negative value) or freezing (positive value) rate and is represented as a vertical velocity at $z = 0$ (see Fig. 2). Also, for small $|W_0/u_\tau|$, vertical advection terms can be neglected in (1a, b), (2) and (3). Later, our calculations will show that $W_0/u_\tau = O(10^{-3})$.

a. Turbulence closure model

The turbulence closure model of Mellor and Yamada (1974, 1982) is embedded in the numerical model; we use the so-called level 2½ version of the closure model. Although one must refer to the papers cited for a complete account of model derivation, we provide brief commentary here in response to reviewer requests.

The closure model begins with the prognostic equations for all six components of the Reynolds stress tensor and for the three components of the heat and salinity (when applied to the ocean) flux vectors. Closure hypotheses for the pressure, velocity gradient correlation tensor (following Rotta, 1951a,b) and the dissipation tensor (following Kolmogorov, 1941) are adopted and extended to similar terms involving density fluctuations. Terms such as those for all stress and flux components and for shear and buoyancy production appear quite naturally and do not require modeling. Turbulent diffusion terms are also modeled but are not of primary importance. Model constants are determined from neutral laboratory data. An early application of the model (Mellor, 1973) yielded Monin–Obkhov similarity relations in close agreement with near-surface, atmospheric boundary layer data. The complete model calling for the solutions of prognostic equations for all stress and flux components was labeled the level 4 model. Mellor and Yamada (1974) then developed a procedure to approximate the full prognostic equation set in order to reduce their number and reduce complexity and computational cost. As summarized by Mellor and Yamada (1982), level 3, 2 and 1 models now exist, but somewhat as an afterthought, a level 2½ was defined and is used here. This requires prognostic equations for q^2, twice the turbulence kinetic energy and $q^2 l$ where l is a turbulence macroscale; it is approximately proportional to the integral of the velocity correlation function and is deliberately scaled so that, adjacent to a surface, it is asymptotically equal to Prandtl's mixing length as the surface is approached. Vertical mixing coefficients for velocity and temperature (or any scalar) are provided by the relation $(K_M, K_H) = lq(S_M, S_H)$. The values S_M and S_H are stability coefficients and are functions of $l^2[\partial U/\partial z)^2 + (\partial V/\partial z)^2]/q^2$ and $l^2 \rho_0^{-1}[\partial \rho/\partial z]/q^2$. Here, ρ is density, defined by an equation of state, $\rho(T, S)$, and ρ_0 is a reference density. It is assumed that the Reynolds and Peclet numbers are very large; a result is that K_H is also the vertical mixing coefficient for salinity and, in fact, for any other scalar property.

b. Surface boundary conditions

In this paper we will provide the option of specifying surface boundary conditions for either ice velocity or interfacial shear stress. The latter option is simplest and we consider it last. We will also need to specify T_0 and S_0 as surface boundary conditions. Note, however, that the model requires boundary information at some arbitrarily small distance away from the surface where the model-generated mixing coefficients and equations (7a, b), (8) and (9) are valid. Therefore, since, $(\tau_x, \tau_y) = K_M(\partial U/\partial z, \partial V/\partial z)$, $F_t = -K_H(\partial T/\partial z)$ and $F_s = -K_H(\partial S/\partial z)$, the surface boundary conditions for (1a, b), (2) and (3) may be obtained from (7a, b), (8) and (9). Thus,

$$ku_\tau \frac{(U_i - U, V_i - V)}{\ln(-z/z_0)} = K_M\left(\frac{\partial U}{\partial z}, \frac{\partial V}{\partial z}\right), \quad -z \to z_0 \tag{10a, b}$$

$$ku_\tau \frac{(T_0 - T)}{\ln(-z/z_{0t})} = K_H \frac{\partial T}{\partial z}, \quad -z \to z_0 \tag{11}$$

$$ku_\tau \frac{(S_0 - S)}{\ln(-z/z_{0s})} = K_H \frac{\partial S}{\partial z}, \quad -z \to z_0. \tag{12}$$

For Eq. (10a, b) we immediately assume that velocity is continuous across the ice–seawater interface so that $(U_0, V_0) = (U_i, V_i)$. Thus, with (U_i, V_i), T_0 and S_0 as input information, Eqs. (10a, b), (11) and (12) provide mixed Neuman–Dirichlet boundary conditions relating $U(z)$, $V(z)$, $T(z)$ and $S(z)$ and their derivatives. Numerically, these boundary conditions are applied to the first grid point, z, nearest the interface where $-z > z_0$. The variables K_M, K_H, T_0 and S_0 are evaluated from the previous time step. Furthermore, $z_0 \approx$ (height of roughness elements)/30. The remaining unknowns in the surface boundary conditions are T_0, S_0, u_τ, z_{0t} and z_{0s} and will be discussed in the following sections.

We will also show results of calculations where, instead of (U_i, V_i), surface stress is the dynamical boundary condition, in which case the surface stress components replace the left sides of (10a, b).

c. Interfacial thermal and salt balance

Figure 1 is a schematic of the equilibrium seawater, ice-phase diagram for a *material* volume, which is a volume enclosed by a *material* surface through which mass flux is everywhere null. Ice supports negligible quantities of salt in its crystalline structure (Weeks and Ackley, 1982), and therefore, the freezing process must be accompanied by salinity flux through the material surface. However, in a not-so-slow, nonequilibrium process, the sea ice can trap brine pockets, and therefore, the average salinity can be nonzero.

We write a heat balance for a vanishingly thin *control* volume—rather than a material volume—surrounding the sea ice–seawater interface. This is illustrated in Fig. 2. Thus,

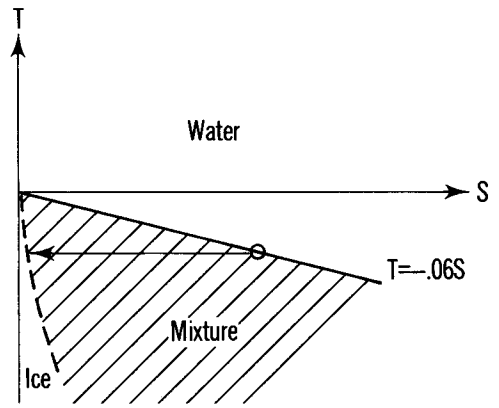

FIG. 1. Equilibrium phase diagram for ice–seawater, delineating regions of seawater, seawater–ice mixture (shaded region) and ice. The areal extent of the latter region is exaggerated; ice crystal structure accommodates only negligibly small concentrations of salt. The solid line is the freezing transition interface whereas the dashed line is the melting transition interface. The horizontal arrow illustrates a constant temperature freezing process for a material volume (enclosed by a material surface through which the mass flux is everywhere zero) that requires heat flux and salt flux out of the material volume.

$$\rho_0 W_0 h_0 + \rho_0 C_{p0} F_t = \rho_i W_i h_i + \rho_0 C_{p0} Q_i$$

where the subscript 0 refers to the seawater side of the interface ($z = 0-$) and i to the sea ice side ($z = 0+$), ρ is density, W the vertical velocity of water crossing the interface, and h the enthalpy. We define $\rho_0 C_{p0} Q_i$ as the heat conduction through the ice and therefore define Q_i in a way that will simplify notation. We now note that $\rho_0 W_0 = \rho_i W_i$ so that

$$W_0 L + F_t = Q_i. \tag{13}$$

We will refer to W_0 as the freeze rate (positive (quantity) or melt rate (negative quantity) although the quantity, $\rho_0 W_0/\rho_i = 1.09 W_0$ is often assigned this definition in the literature. In (13) sensible heat has been neglected so that $h_0 - h_i$ is the heat of fusion, which we approximate as $L \equiv (h_0 - h_i)/c_{p0} = 80°\text{C}\,(1 - S_i/S_0)$, where S_i is the average salinity of the ice; the factor $(1 - S_i/S_0)$ approximately accounts for brine pockets in the ice, assuming that the pockets were trapped at the salinity, S_0.

Again referring to Fig. 2, we write a salt balance according to

$$F_s = W_0(S_i - S_0). \tag{14}$$

If F_t and F_s are eliminated from (8) and (9) using (13) and (14), we obtain

$$T_0 - T = \frac{W_0 L - Q_i}{ku_\tau} \ln \frac{-z}{z_{0t}} \tag{15}$$

$$S_0 - S = W_0 \frac{(S_0 - S_i)}{\text{ku}\tau} \ln \frac{-z}{z_{0s}}. \tag{16}$$

The final equation is the freezing transition interface

$$T_0 = mS_0; \quad m = -0.06°\text{C}/(‰). \tag{17}$$

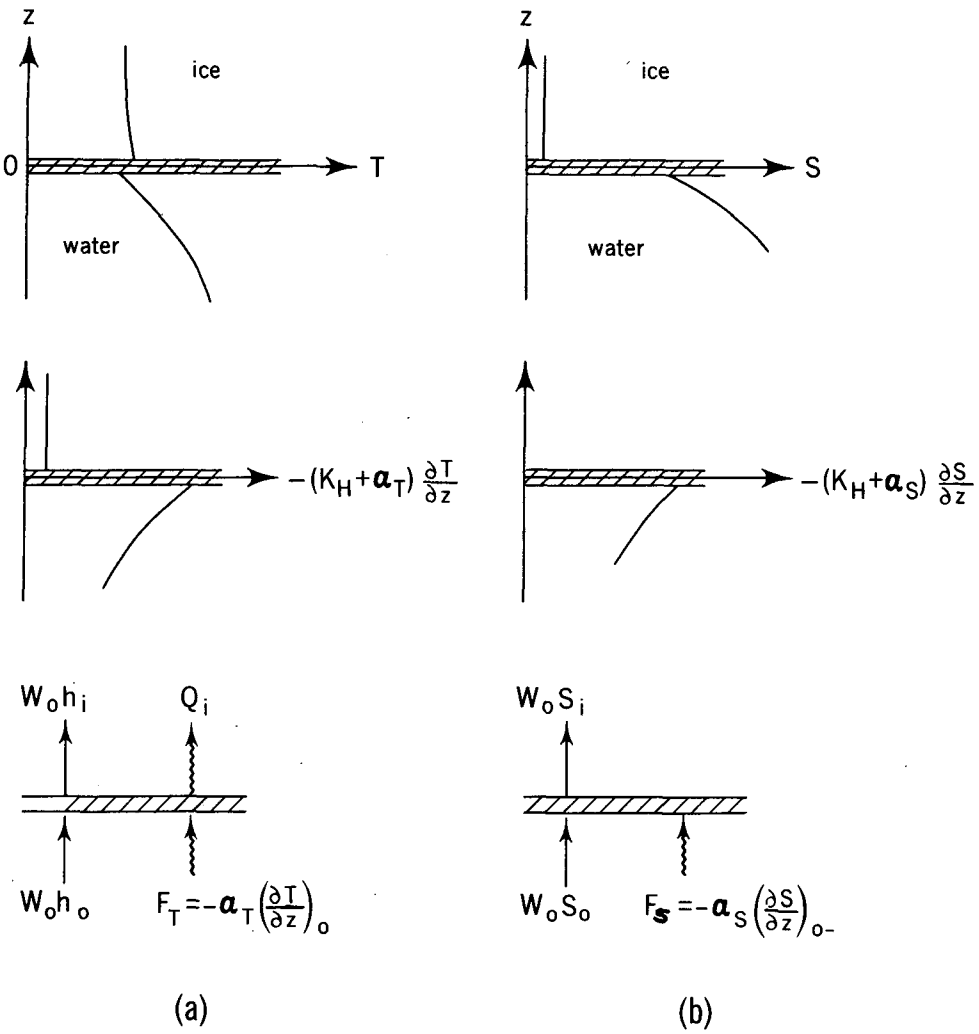

FIG. 2. Schematic of the properties (upper panels), fluxes (middle panel) and interfacial advection and flux balance (lower panel) for (a) temperature and (b) salinity. The subscript i denotes values on the ice side at $z = 0+$ whereas the subscript 0 denotes values on the water side at $z = 0-$. The shaded portion represents an indefinitely thin control volume surrounding the seawater, sea-ice interface.

Thus, given T, S at z (numerically taken as the nearest grid to the surface where $-z > z_0$) and also Q_i and S_i, then (15), (16) and (17) can be solved for T_0, S_0 and W_0. An equation for T_0 or S_0 is obtained by combining the three equations; the result is

$$T_0 = mS_0$$

$$= \frac{LR + mS_i + \tilde{T} - [LR + mS_i + \tilde{T})^2 - 4m(\tilde{T}S_i + LRS)]^{1/2}}{2} \quad (18a)$$

where

$$\tilde{T} \equiv T - \frac{Qi}{ku_\tau} \ln\left(\frac{-z}{z_{0t}}\right) \quad (18b)$$

$$R \equiv \frac{\ln(-z/z_{0t})}{\ln(-z/z_{0s})}. \quad (18c)$$

Equation (18a, b, c) may be used in conjunction with (10a, b), (11) and (12) to provide the interfacial boundary conditions and (4a, b), (5) and (6), the free-stream boundary conditions, as (1a, b), (2), (3) are integrated forward in time. The melting or freezing rate is found diagnostically from either (15) or (16).

d. *The roughness parameters*

For sufficiently rough surfaces, z_0 is related to the actual height of roughness elements and is not a function of molecular viscosity. This is due to the fact that Reynolds stresses away from the surfaces are equal to surface integrals of the component of pressure acting normal to the rough surface in the mean flow direction. Since this *form drag* has no counterpart in scalar equations, the flux of temperature or salinity must reduce

to molecular diffusion at solid surfaces where the normal component of turbulence velocity is null. Note that the representation, $F_T = -\alpha_t(\partial T/\partial z)_{0-}$ in Fig. 1 is simplistic. The right side should more accurately be written as a surface integral of $-\alpha_t \partial T/\partial n$ over the rough surface divided by the area projected on a z-plane; here $\partial T/\partial n$ is the temperature gradient normal to the rough surface. In view of this, one supposes that $z_{0t} = \text{fcn}(\alpha_t, u_\tau, z_0)$ or $z_{0t}u_\tau/\alpha_t = \text{fcn}(z_0 u_\tau/\alpha_t)$. A similar form can be written for z_{0s}. Sverdrup (1951) and Sheppard (1958) suggested the simplest possible forms for scalar properties, which in the present application are

$$z_{0t} = \frac{\alpha_t}{k u_\tau} \tag{19}$$

$$z_{0s} = \frac{\alpha_s}{k u_\tau}, \tag{20}$$

and may be obtained by assuming that the molecular and turbulence diffusivities are additive so that, for example, $F_H = -(K_H + \alpha_t)\partial T/\partial z$ where $K_H = k u_\tau z$ and then integrating from $z = 0$ to an arbitrary depth while holding F_H constant. This seems overly simplistic, but Garrett and Hicks (1973) after examination of considerable data find (19) acceptable.

Since $\alpha_t = 1.31 \times 10^{-7}$ m^2 s^{-1} and $\alpha_S = 7.40 \times 10^{-10}$ m^2 s^{-1} and for, say, $u_\tau = 0.01$ m s^{-1}, typical values are $z_{0t} = 3.27 \times 10^{-5}$ m and $z_{0s} = 1.85 \times 10^{-7}$ m.

e. *Steady, inhomogeneous boundary layers*

For steady, two-dimensional boundary-layer development, wherein properties are invariant in the y-direction, the governing equations are

$$\frac{\partial U}{\partial x} + \frac{\partial W}{\partial z} = 0 \tag{21}$$

$$U\frac{\partial U}{\partial x} + W\frac{\partial U}{\partial z} - fV = -fV_g + \frac{\partial}{\partial z}\left(K_M \frac{\partial U}{\partial z}\right) \tag{22a}$$

$$U\frac{\partial V}{\partial x} + W\frac{\partial v}{\partial z} + fU = fU_g + \frac{\partial}{\partial z}\left(K_M \frac{\partial V}{\partial z}\right) \tag{22b}$$

$$U\frac{\partial T}{\partial x} + W\frac{\partial T}{\partial z} = \frac{\partial}{\partial z}\left(K_H \frac{\partial T}{\partial z}\right) \tag{23}$$

$$U\frac{\partial S}{\partial x} + W\frac{\partial S}{\partial z} = \frac{\partial}{\partial z}\left(K_H \frac{\partial S}{\partial z}\right) \tag{24}$$

where (U_g, V_g) is the (constant) geostrophic velocity. Flow under fast ice is considered so that the ice velocity is zero. As $z \to -\infty$ we have $U \sim U_g$, $V \sim V_g$. Figure 3 is a sketch of the flow.

A good approximation to the above equation set is

$$U_g\frac{\partial U}{\partial x} - fV = -fV_g + \frac{\partial}{\partial z}\left(K_M \frac{\partial U}{\partial z}\right) \tag{25a}$$

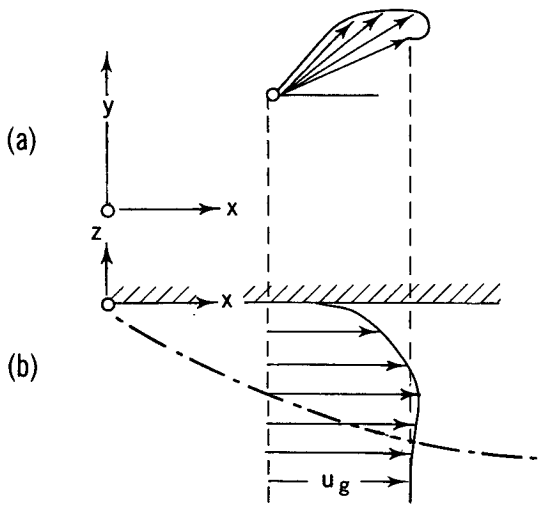

FIG. 3. Schematic of steady boundary layer growth under stationary ice. Solutions for this case may be obtained from the unsteady horizontally homogeneous solutions via the transformation cited at the end of section 2. (a) Hodograph of the layer profile. (b) Projection of the profile on a vertical plane normal to the ice leading edge. The dotted–dashed curve signifies growth of the layer thickness.

$$U_g\frac{\partial V}{\partial x} + fU = fU_g + \frac{\partial}{\partial z}\left(K_M \frac{\partial V}{\partial z}\right) \tag{25b}$$

$$U_g\frac{\partial T}{\partial x} = \frac{\partial}{\partial z}\left(K_H \frac{\partial T}{\partial z}\right) \tag{26}$$

$$U_g\frac{\partial S}{\partial x} = \frac{\partial}{\partial z}\left(K_H \frac{\partial S}{\partial z}\right). \tag{27}$$

The physical reason why these equations are a good approximation to (22a, b), (23) and (24) is that turbulent profiles do not vary greatly except very close to surfaces. [It turns out that the approximation is quite good even for laminar boundary layers; for example, compare the Raleigh solution and the Blasius solution (Schlicting, 1975): the profiles are quite similar and the growth rates differ by about 25%.] For turbulent boundary layers Mellor (1972) shows that the approximation is exact in the limit of infinite Reynolds number. The point of this is that all of the solutions obtained according to (1a, b), (2), (3), (4a, b), (5), (6), (10a, b), (11) and (12) apply to the above equations such that, if we assign asterisks to the variables in (25a, b), (26) and (27), $x^* = U_g t$, $U_g \partial(\ )/\partial x^* = \partial(\ )/\partial t$ and $(U,^* V^*) = (U + U_g, V + V_g)$.

3. Model calculations

For all of the cases discussed in this section the initial salinity is set at the constant value, 34‰ above 50 m; below 50 m a halocline is established. This is below the depth of significant stress penetration ($\sim 0.5u_\tau/f$) for any of the surface stress values that we will encounter in this paper. In fact, when melting is enabled, wind-stress penetration will be further inhibited, as we

see shortly. The calculation is actually carried down to a depth of 80 m. We use a vertical grid with 100 grid points with closer spacing near the surface. The integrating time step is 15 min. This resolution is much more than necessary; halving the number of grid points or doubling the time step produced negligible change. However, so long as the calculations are one-dimensional, the computational costs of fine resolution are not of consequence.

The surface will be forced by both surface (ice) velocity and stress, where, in both cases, only the x-component will be nonzero. Rigorously, it is only in the former case that the transformation, discussed in section 2, can be applied without approximation; in the latter case, one must be willing to approximate the resultant ice velocity as a constant to effect the transformation.

The ice velocity or interfacial stress will be ramped up from zero over one inertial period and held constant thereafter; it can be shown that this results in minimal inertial oscillations due to the start-up process.

a. The case of zero melt/freeze rate

The case of zero melt rate can be obtained by setting $Q_i = 0$ and by setting the initial temperature at -2.04°C. This thermodynamic state is located on the freezing transition interface in Fig. 1. With vertical homogeneity and no melting or freezing, vertical density gradients will be null and boundary-level turbulence will not be influenced by gravity.

We first force the flow with ice velocity which, after the first inertial period, is (0.20, 0.0) m s^{-1}. Figure 4 depicts the evolution of velocity, twice the turbulence kinetic energy and the vertical eddy viscosity.

We have also calculated the case where the flow is forced by an imposed surface stress. Since the surface velocity is, after the start-up period, very nearly constant in time, the velocity-forced case and the stress-forced case are nearly equivalent for the same stress modulus except for details near time = 0. Figure 5 shows plots of drag coefficient defined as the surface stress vector modulus divided by the square of the ice

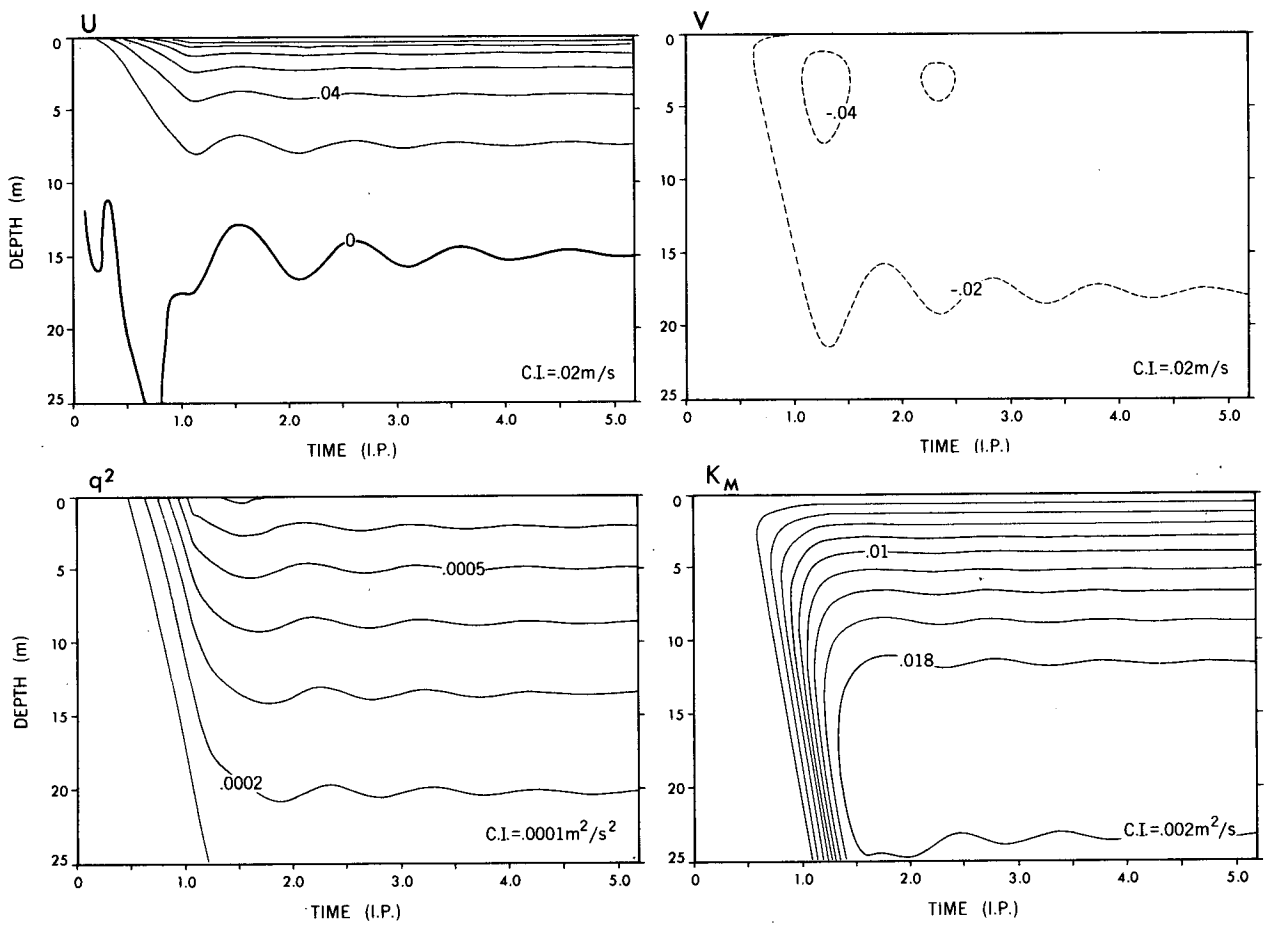

FIG. 4. Boundary layer development for zero melt/freeze rate where the initial temperature is constant at -2.04°C. Above 50 m the salinity is constant at 34‰; below 50 m a stable halocline is established. The flow is forced by an imposed ice velocity, which is ramped up from zero through one inertial period and then held constant at the value, (U_i, V_i) = (0.20, 0.0) m s^{-1}. The top panels are the velocity components. The bottom panels are twice the turbulence kinetic energy and the vertical eddy viscosity. The temperature and salinity fields are unchanged from their initial values.

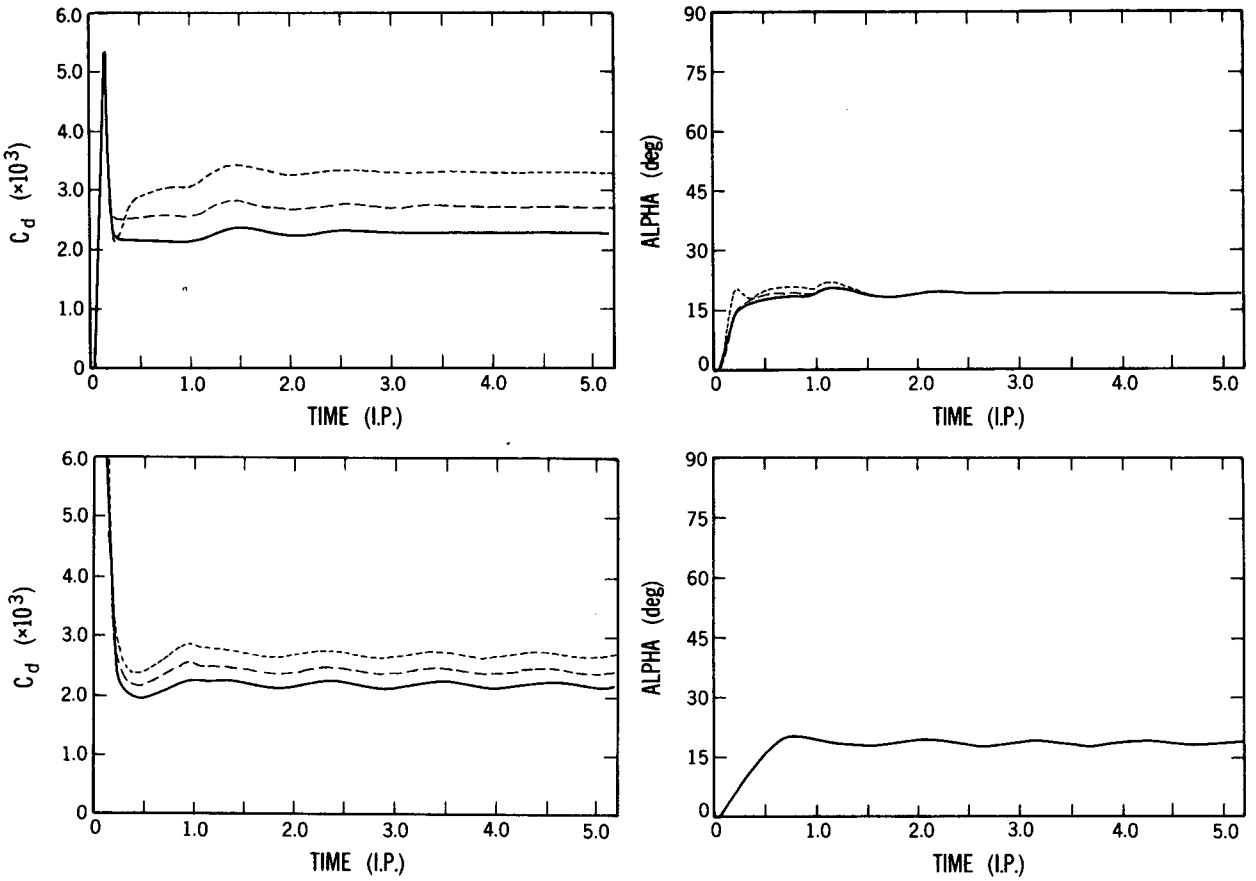

FIG. 5. The drag coefficient and the angle between the surface stress and the ice velocity vectors when the initial temperature is −2.04°C. The top panels correspond to Fig. 4 (long dashed lines), where we also include surface velocities of 0.10 (short dashed lines) and 0.40 (solid lines) m s^{-1}. The bottom panels correspond to cases forced by surface stresses of 1.0 (short dashed lines), 2.0 (long dashed lines) and 4.0 (solid dashed lines) cm^2 s^{-2}.

velocity vector modulus and the angle between the stress and the ice velocity vector, the so-called veering angle. The top panel are results for the surface velocity-forced calculations whereas the bottom panels are the surface stress-forced calculations. The differences are small, unlike the corresponding, stratified cases discussed below. For steady, neutral flow, the drag coefficient and veering angle may be reduced to

$$C_d = k^2\{[\ln(u_\tau/fz_0) - A]^2 + B^2\}^{-1} \quad (28)$$

$$\alpha = \tan^{-1}\{B/[\ln(u_\tau/fz_0) - A]\}. \quad (29)$$

The present model produces neutral profiles where A = 1.8 and B = 2.3. Thus, the variations in C_d seen in Fig. 5 are due to variations in the parameter, u_τ/fz_0.

b. *Cases of nonzero melt rate*

Figure 6 depicts a case where the initial conditions are the same as before except that the initial temperature is 0.0°C and therefore warmer than the freezing transition temperature. We again drive the flow by setting the ice velocity (U_i, V_i) at the value, (0.20, 0.0) m s^{-1}, after the previously described ramping process. We contrast these results with the case in Fig. 7 where the kinematic, surface stress, (τ_x^0, τ_y^0), is ramped and then set to the final value, (2.0, 0.0) cm^2 s^{-2}. In all cases melting was delayed for two inertial periods to allow for the establishment of a very nearly steady flow. We envision that this procedure will approximate a sharp front of warm water moving under an ice edge or ice moving over a stationary warm front. In either case the procedure will have established an initial wind-driven mean velocity and turbulence field in the water column in a simple way. This is idealized input to the problem but, nevertheless, input resulting in a response that is easily comprehended.

Drag coefficients, veering angles and melt rates, normalized on u_τ, corresponding to Figs. 6 and 7, are shown in Figs. 8 and 9, respectively. We also include in the latter figures a range of surface forcing values and cases for an initial temperature of 2.0°C.

Prior to the initiation of melting, the turbulence energy and mixing coefficients are relatively large. Then,

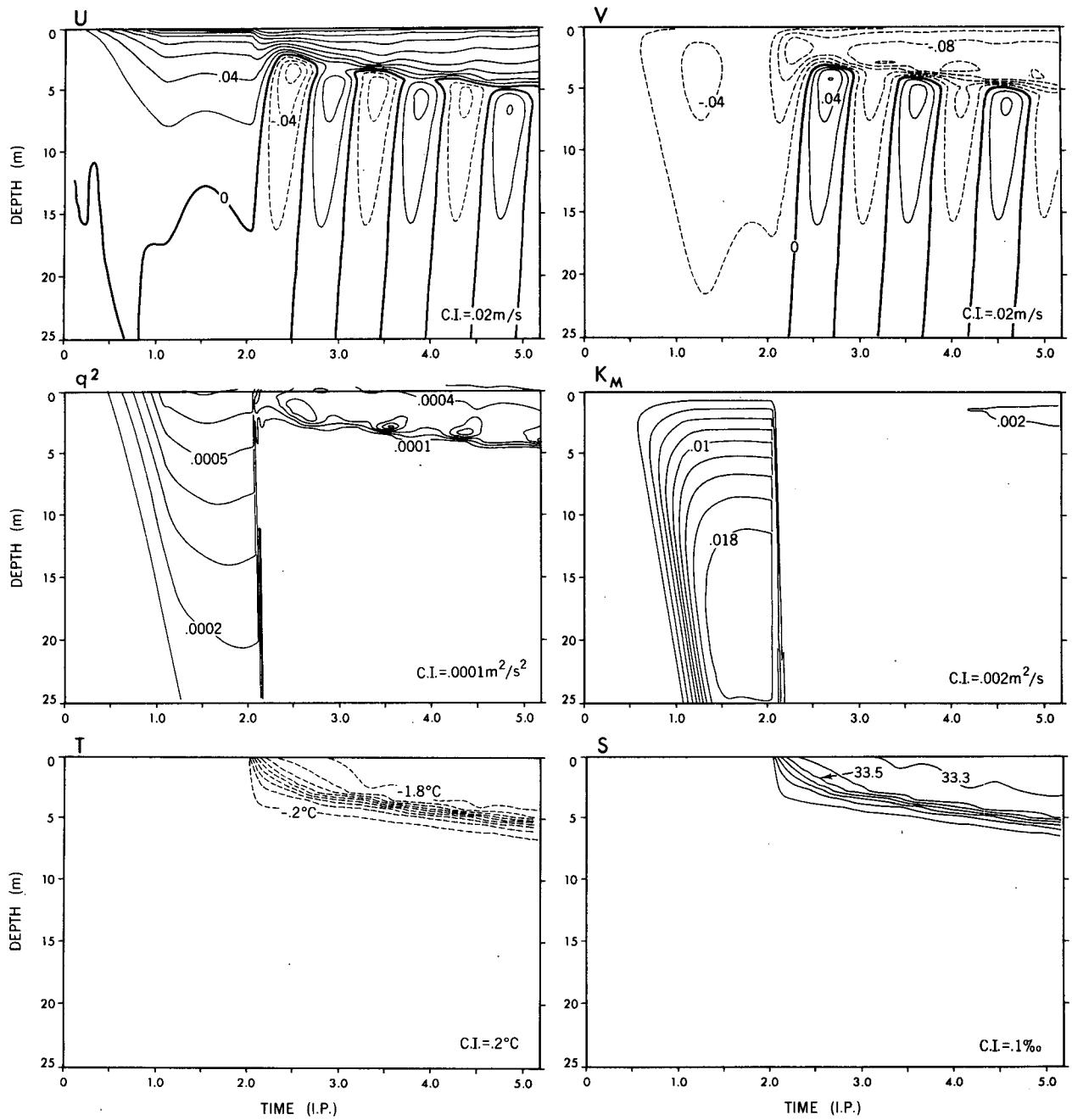

FIG. 6. Boundary layer development with melting ice where the initial temperature is 0.0°C. The flow is forced by an imposed surface (ice) velocity, ramped up from zero through one inertial period and then held constant at the value $(U_i, V_i) = (0.20, 0.0)$ m s^{-1}. Melting is enabled after two inertial periods. The top panels are the velocity components. The middle panels are twice the turbulence kinetic energy and the vertical eddy viscosity. The bottom panels are temperature and salinity.

melting creates a surface buoyancy flux and a new, much shallower mixed layer. The differences in mixed-layer depth in Figs. 6 and 7 are primarily due to the fact that, in the former case, $u_\tau^2 = 1.1$ cm^2 s^{-2} and decreases after melting begins (see C_d in Fig. 8), whereas $u_\tau^2 = 2.0$ cm^2 s^{-2} in the latter case. In both cases the mixing coefficients are reduced from the neutral values due to decreases in the turbulence energy, the turbulence length scale and the stability factor, S_M. Melt rates are similarly reduced.

A striking feature of both Figs. 6 and 7 is the creation of inertial oscillations; however, in Fig. 6, the oscillations occur only below the newly created, stable pycnocline whereas, in Fig. 7, they occur above and below.

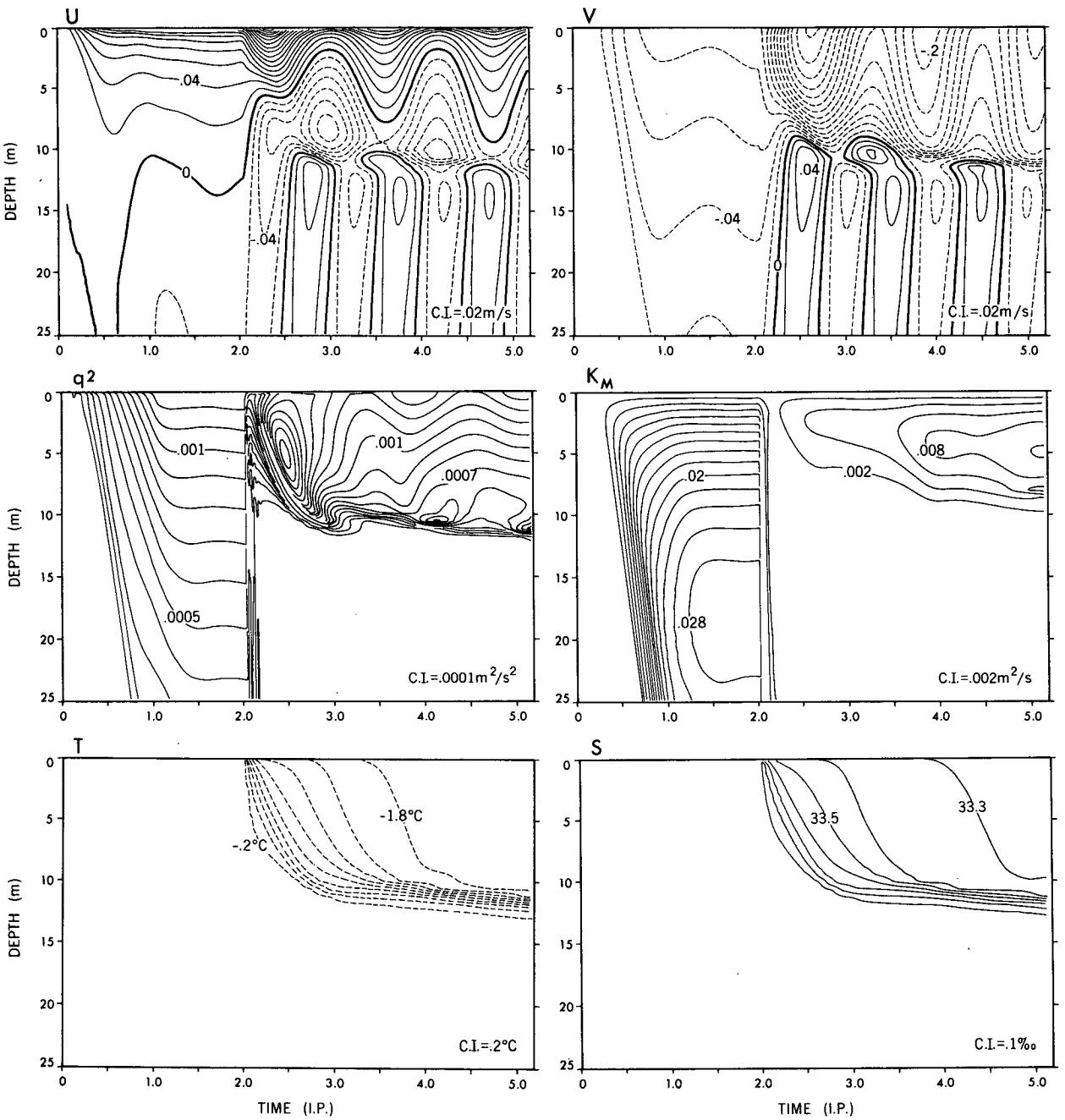

FIG. 7. As in Fig. 6 but for the flow forced by an imposed surface stress velocity, ramped up from zero through one inertial period and then held constant at the value $(\tau_x^0, \tau_y^0) = (2.0, 0.0)$ cm^2 s^{-2}.

To explain these behaviors we refer to the equations of motion in complex form, $\partial\tilde{u}/\partial t - if\tilde{u} = \partial\tilde{\tau}/\partial z$, where $\tilde{u} \equiv U + iV$ and $\tilde{\tau} \equiv \tau_x + i\tau_y$.

Below the newly established pycnocline, the mixing coefficient, and therefore $\partial\tilde{\tau}/\partial z$, decreases to zero in a time interval much shorter than an inertial period. Assuming an instantaneous decrease, the solution is $\tilde{u}_0 \exp[if(t - t_0)]$ where $\tilde{u}_0$ and t_0 are the initial velocity and time at the time of the decrease in shear-stress gradient.

Above the new pycnocline, in the case of Fig. 7, the surface stress is unchanged but the stress at the new pycnocline has very nearly vanished; therefore, the shear-stress gradient increases. The same analytical solution prevails here with the addition of a complex constant and with an appropriate $\tilde{u}_0$.

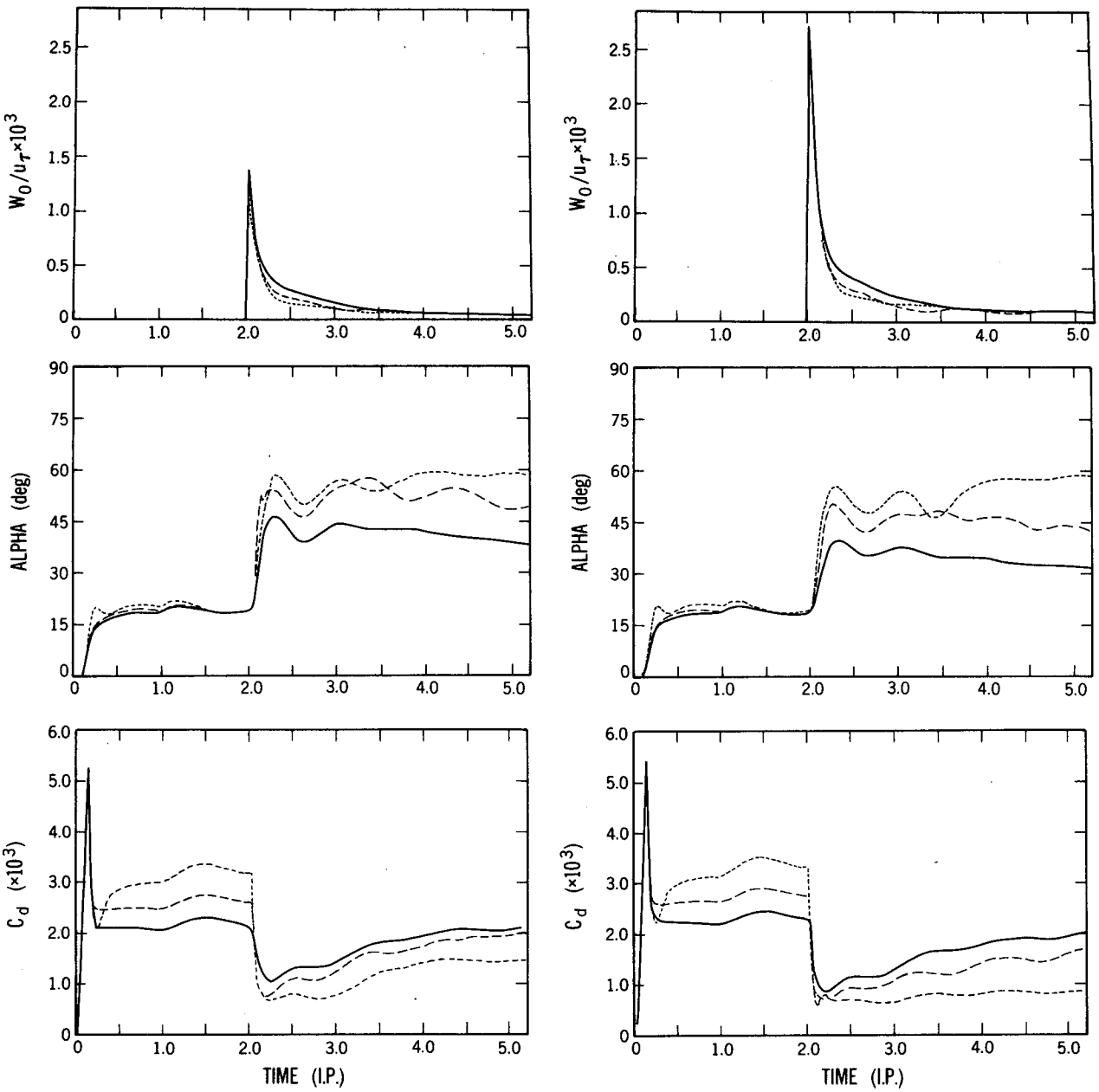

FIG. 8. The drag coefficient and angle between the surface stress and ice velocity vectors and the melt rate normalized on u_* corresponding to Fig. 6 (long dashed lines). Also included are cases for imposed surface velocities of 0.10 (solid lines) and 0.40 (short dashed lines) m s^{-1}. The panels on the left are for initial temperature of 0.0°C whereas the panels on the right are for 2.0°C.

Above the pynocline, in the case of Fig. 6, the surface velocity is held constant; the subsurface velocities are also approximately constant so that inertial oscillations are precluded. This requires that the surface stress decrease to maintain a nearly constant shear-stress gradient.

This single-frequency, inertial motion is idealized, of course, due to impulsive initiation of melting and the assumption of horizontal homogeneity. Nevertheless, the basic mechanism is likely to prevail in nature; it is a process related to the nocturnal jet in the atmospheric boundary layer.

c. *The freezing process*

To examine a freezing case, the model was initialized as it was in the case of no melting or freezing; i.e., the initial thermodynamic state is located on the freezing line and the flow is dynamically forced by ice velocity = (0.20, 0.0) m s^{-1}. To produce freezing, heat con-

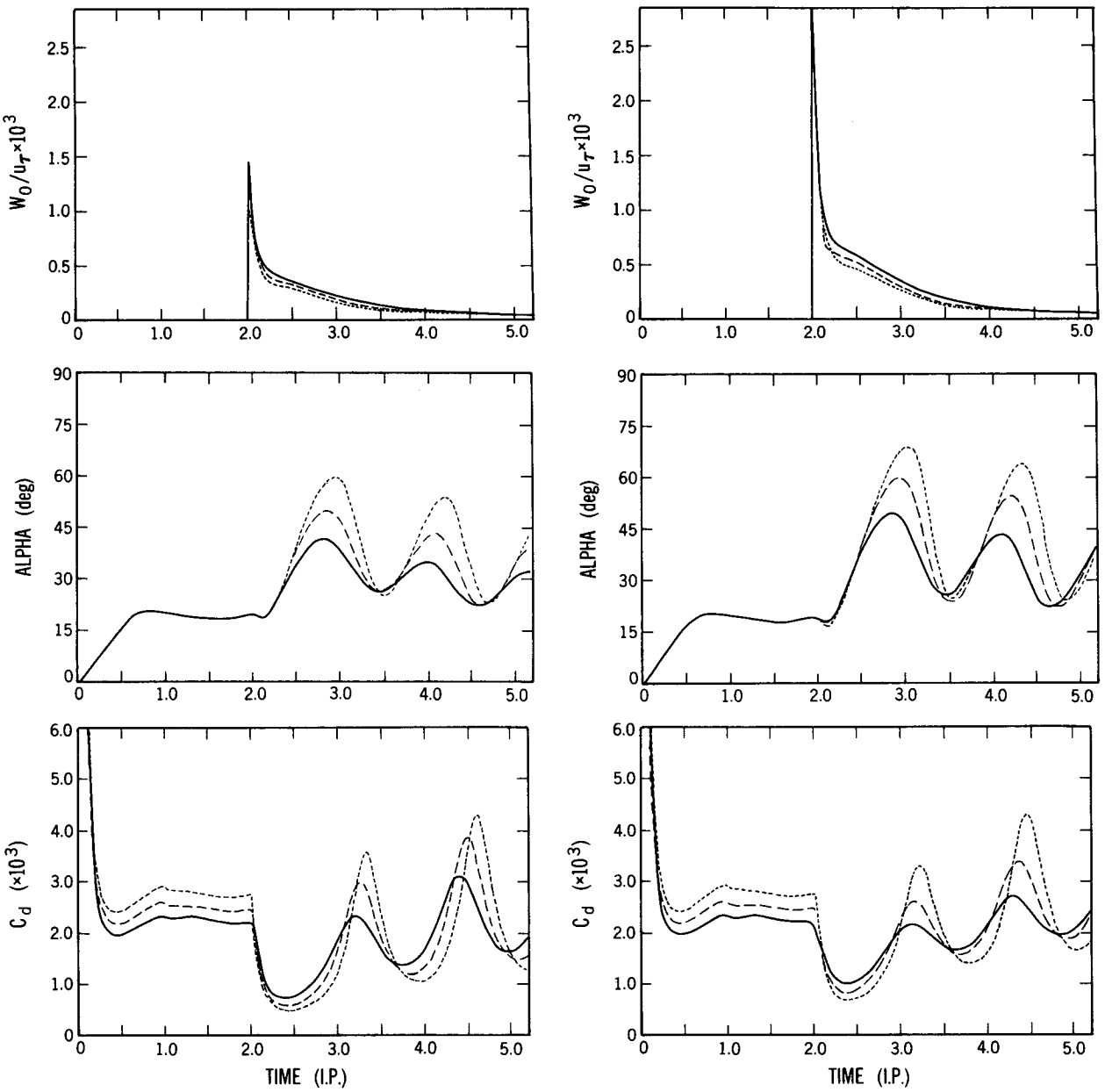

FIG. 9. As in Fig. 8 but corresponding to Fig. 7. Also included are cases for imposed surface stresses of 1.0 (short dashed lines) and 4.0 (solid lines) cm^{-2} s^{-2}.

duction through the ice is specified as $\rho_0 C_{p0} Q_i = 60$ W m^{-2}. This rate is typical of that found due to atmospheric and radiational, wintertime cooling but is very much smaller in absolute magnitude than the heat fluxes obtained from the melting ice calculations.

Results of the calculations are shown in Fig. 10. Here we show greater depths to emphasize that the flow is weakly unstable and the turbulence penetrates to the top of the pynocline, which is slowly eroded. On the time scale of this calculation the mean velocity does not differ greatly from the neutral case of no melting or freezing even though the mixing coefficient is significantly increased in the middle of the layer; there, the velocity profiles are fairly flat.

In the previous melting cases we had set Q_i equal to zero so that the heat flux, F_s, and salt flux, F_t, were linearly related to the melt rate as described by (13) and (14). In the present freezing simulation, F_t is a negligible fraction of Q_i since the ice temperature and the temperature of the water column are very close. Therefore, the freeze rate, W_0, is constant at 1.46 cm d^{-1}.

Throughout the mixed layer the calculations produced a small amount of supercooling, implying the

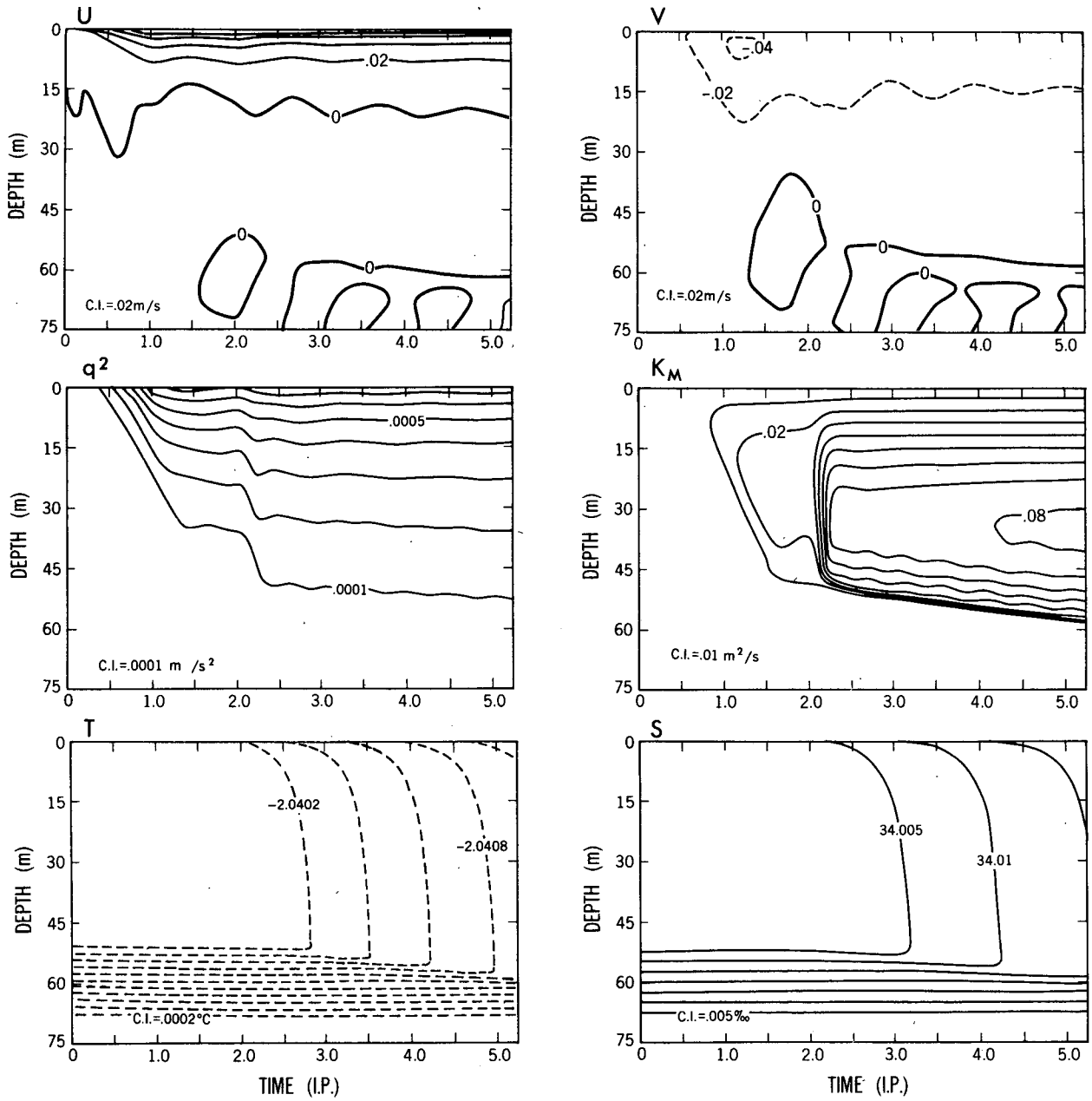

FIG. 10. Boundary layer development for freezing ice where the initial temperature is constant at −2.04°C. Above 50 m the salinity is constant at 34‰; below 50 m a stable halocline is established. The flow is forced by an imposed ice velocity, which is ramped up from zero through one inertial period and then held constant at the value, $(U_i, V_i) = (0.20, 0.0)$ m s^{-1}. Heat conduction through the ice at the rate of 60 w m^{-2} is imposed after two inertial periods. The top panels are the velocity components. The middle panels are twice the turbulence kinetic energy and the vertical eddy viscosity. The bottom panels are temperature and salinity fields.

creation of frazil ice. The process may be understood as follows. Over the domain of the model the average change in salinity is the time integral of the surface salinity flux, since there is no flux at the bottom. Similarly, the average change in temperature is the time integral of kinematic heat flux. If the entire water column started at its (surface) freezing point, it will remain on the freezing line if the ratio of surface fluxes, $\langle w'T' \rangle_0 / \langle w'S' \rangle_0$, is equal to m. This will be true only if the eddy diffusivities and surface roughnesses for heat and salt, z_{0t} and z_{0S}, are equal. In the model, the temperature surface roughness is larger than the salinity roughness, which means that across the surface layer heat is transported faster than salt, supercooling the water column. The effect is small. In these calculations, if the supercooled water were restored to equilibrium,

the amount of frazil production amounts to only a half percent of the total. We tried several simulations in which we also varied the ratio of salinity diffusivity to heat diffusivity in the range 0.25 to 1.0, obtaining a maximum supercooling between 0.003° and 0.004°C. Nevertheless, the question may be more than purely academic. Lewis and Perkin (1983) document a number of cases in which the upper boundary layer of the Arctic Ocean was supercooled (relative to surface freezing temperature) by as much as 0.006°C. They attributed the phenomenon to melting of pressure ridge keels at depths where the actual freezing point is depressed relative to the surface by about the observed amount. While that explanation seems plausible, our work indicates that, if turbulence is slightly more efficient at transporting heat than salt, an additional supercooling tendency will occur even under flat ice.

There is considerable interest in frazil ice formation, since it appears that a large percentage of Antarctic sea ice is consolidated frazil (Gow et al., 1982; Clarke and Ackley, 1984). At this time, we do not understand this finding. It is possible that the ice formation at the ice–sea boundary of our model, which we conceive of as being congelated ice, is, in reality, frazil ice.

Omstedt and Svennson (1984) model frazil production in brackish water with a direct air–sea interface and carry their calculations to the point where a solid cover begins to form, which is about where we start. Another important distinction between the problems is that because the salinity in their case is small, their regime is stabilized by freezing rather than destabilized by salt flux. In appendix B, we show how the model may be generalized to include dynamic formation of ice concentration.

4. Ice drift observations and model calculations

In this section we apply the one-dimensional, ocean boundary layer, ice model to the interpretation of a remarkable set of measurements made in the Bering Sea marginal ice zone during March 1981 by Martin et al. (1983; henceforth referred to as MKP). We briefly recap the observations here. Two buoys equipped with radar transponders were initially positioned near the ice edge (which was reasonably well defined at the time) and then tracked by ship's radar for about a day and a half. During this time a limited band of ice, on which the buoys lay, diverged from the edge and eventually melted some distance seaward of the main pack in water well above its freezing point. During most of the time of the monitored drift, winds were north-northeasterly with fairly steady speed.

By comparing positions with another buoy deployed about 80 km farther into the pack, and by considering wind/ice drift characteristics reported by McPhee (1982) for the central Arctic, MKP showed that the ice carrying the buoys drifted faster than ice in the interior would normally drift under the same wind conditions. They hypothesized that wave radiation pressure acting on the upwind (iceward) edge of the band caused its acceleration. Wadhams (1983) proffered essentially the same explanation for this commonly observed ice-edge divergence under the action of off-ice winds. Alternatively, McPhee (1983) suggested that ice-edge divergence in water above its freezing point was mainly due to stabilization of the ocean boundary layer caused by rapid melting, and he formulated a steady state, analytic similarity model for the ice–ocean boundary layer to show that conditions in the Bering could lead to the observed divergence. Josberger (1983), to the contrary, argued that boundary layer stability was unaffected by ice melting even when extreme turbulent heat flux at the navifacial interface caused rapid ice melt. However, we have already seen that melting does induce stabilization.

Specifically, we now show that the time-dependent, numerical model described in this paper corroborates McPhee's hypothesis in that PBL stabilization from ice melt can account for much of the divergence in the MKP data. Although the one-dimensional model applied to an inherently two- or three-dimensional system like the marginal ice zone obviously fails to address a number of important questions, it is, we believe, possible to show that the buoyancy mechanism is important in determining stress (in addition to its importance in determining melt rate).

The problem is best posed by considering the actual drift monitored by MKP (see their Fig. 6 for the buoy trajectories) and the wind measured at the nearby research vessel. Using the complex demodulation procedure described by McPhee (1984), we fitted radar position fixes for buoy velocity, then removed the semidiurnal clockwise and counterclockwise tidal motions. Total and filtered fitted velocity for buoy KURT are shown in Fig. 11, for the period 67.0 to 68.75 (i.e., 0000 GMT on 8 March 1981 to 1800 GMT on 9 March 1981). The drift of buoy JERAL was essentially similar. The complex demodulation requires end segments of approximately 6 hours each, so in what follows we consider the 30-hour period from 67.25 to 68.5.

Ice-edge divergence is shown in Fig. 12a. The vector marked "I" is the displacement of buoy KURT (with tidal effects removed) from day 67.25 to 68.5. The vector "W" is the average wind during the period, shown as an accumulated displacement divided by 50; a common rule of thumb, corroborated by numerous observations, is that pack ice drifting freely (with no internal stress gradients) in the central Arctic Basin drifts at about 2% of the surface wind speed. If this were the case in Fig. 12, "I" and "W" would be of equal length. Finally, the vector marked "fd" is the integrated displacement from hourly calculations of the "freedrift" force balance,

$$\rho_i h f(U_i, -V_i) = \rho_a C_{10} |\mathbf{U}_a| (U_a, V_a) - \rho_0 (\tau_x, \tau_y) \quad (30a)$$

$$(\tau_x, \tau_y) = C_d |\mathbf{U}_i| (U_i \cos\alpha + V_i \sin\alpha, V_i \cos\alpha - U_i \sin\alpha). \quad (30b)$$

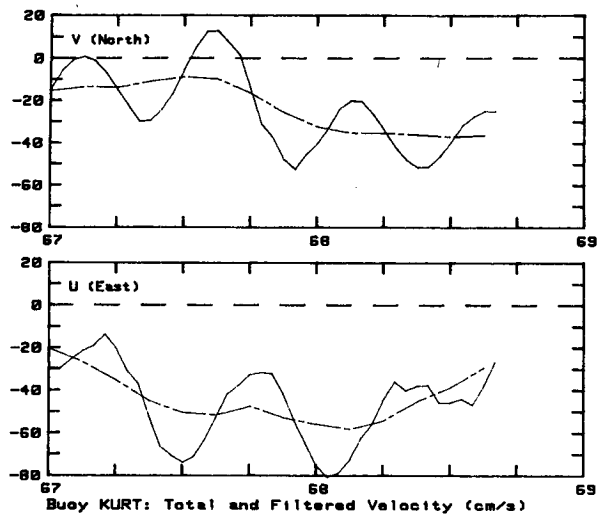

FIG. 11. Buoy KURT velocity components (in cm s^{-1}) for the period, day 67 to 69. Solid lines are fitted velocity assuming clockwise and counterclockwise semidiurnal tides; dashed lines are velocity with tidal components removed.

In the above equations ρ_i, ρ_a and ρ_0 are ice, air and water densities; (U_i, V_i) is the ice velocity vector relative to underlying geostrophic flow and $|\mathbf{U}_i|$ its modulus; (U_a, V_a) is the 10 m wind vector and $|\mathbf{U}_a|$ its modulus; h is ice thickness and f the Coriolis parameter; C_{10} is the surface wind drag coefficient. The drag coefficient, C_d, and veering angle, α, are obtained from Eqs. (28) and (29) wherein z_0 is the under-ice roughness length; for this calculation the values $A = B = 2.0$ were used based on summertime drift observations from the central Arctic during AIDJEX. We have also used the empirical combination of $C_{10} = 0.0027$ and $z_0 = 10$ cm, which was found to be appropriate to the AIDJEX study.

To this point, the analysis of MKP parallels the development here; however, they extrapolated from the Rossby similarity stress–velocity relation to reason that, since the ice was moving rapidly, the stress at the ice–ocean interface must be large relative to the wind stress, requiring a residual term in the balance of forces acting on the ice. They attributed this residual to surface wave radiation stress.

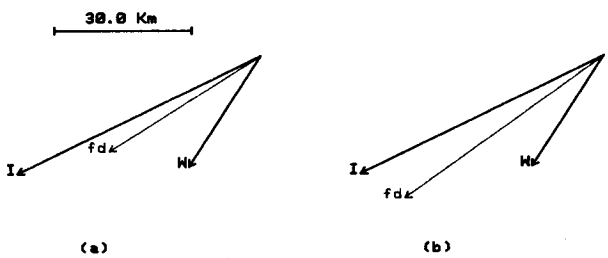

FIG. 12. Ice displacement (I) and integrated wind displacement divided by 50 (W) for the period 67.25 to 68.5, along with integrated free-drift displacement for (a) $z_0 = 10$ cm, and (b) $z_0 = 1$ cm.

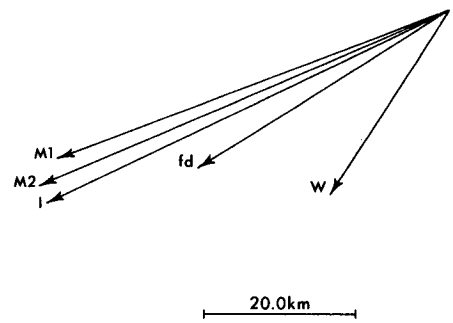

FIG. 13. Wind, ice and free-drift displacements as in Fig. 12a, along with calculated model surface (ice) displacements. M1 is with z_0 constant (10 cm); M2 is with $z_0 = 10$ cm at day 67.75, decreasing to 1 cm at day 68.25 and thereafter maintained constant.

Suppose, instead, that the characteristics of the turbulent boundary layer change at the ice edge so as to reduce oceanic drag. In that case, the ice will drift more rapidly. A plausible candidate for reduction in oceanic boundary layer drag is smoothing of the under-ice surface by melting. Figure 12b is like Fig. 12a except that the under-ice surface roughness, z_0, is equal to 1 cm instead of 10. This produces the right magnitude of drift, without some of the objections of the wave radiation stress argument (e.g., failure to account for form drag force on the leading edge as a floe moves relative to the underlying boundary layer). However, it overlooks two important observational facts: 1) the ice not only moves faster than interior ice, it also deflects farther to the right of the surface wind; and 2) it melts rapidly.

The first observation is difficult to reconcile with reducing drag merely by reducing the size of roughness elements. Rossby scaling of the boundary layer shows

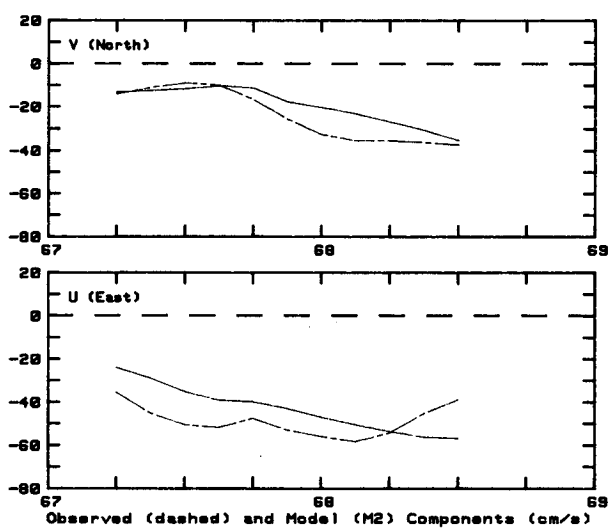

FIG. 14. Smoothed model (M2) surface velocity components compared with smoothed observed velocity (in cm s^{-1}).

that as the surface roughness scale decreases relative to the natural boundary layer scale, both drag and veering decrease. This is evident in Fig. 12 (see also Figs. 8 and 9) where the turning angle for the free drift displacement is less in case b. The increased deflection angle is also hard to explain if one invokes enhanced forcing from wave radiation stress, or from higher wind stress. Either force would align with the surface wind and would tend to reduce the drift angle.

The importance of rapid ice ablation is that surface buoyancy flux is proportional to melt rate and, by analogy with other planetary boundary layers, buoyancy will have a major impact on PBL dynamics (McPhee, 1981, 1983).

Using wind measured during the Bering Sea experiment, we simulated the ocean boundary layer with the one-dimensional model described in section 2. For consistency with the previous free-drift calculations, we specified the 10 m wind drag coefficient as 0.0027. Equation (30a) again represents the ice dynamics. However, in this calculation the drag relation between the interfacial stress and the ice velocity is obtained from the model and not from (30b).

For surface roughness, we considered two cases. In the first case, we held z_0 constant at 10 cm, again to be consistent with the previous free-drift treatment. In the second case, we decreased z_0 linearly from 10 to 1 cm during the same interval of time period when the water column was warmed; our reasoning is that rapid melting would significantly smooth jagged pack ice edges and reduce its large apparent roughness.

The model was initialized as follows. Ice thickness was set at 1.5 m. Water column salinity was set to 32‰ in a 40-m deep mixed layer, below which a constant salinity gradient was specified so that the Brunt-Väisälä frequency was 0.02 s^{-1}. Temperature was set uniformly to the mixed-layer freezing point. To simulate with the one-dimensional model the effect of ice drifting over water that is above the freezing temperature, we uniformly heated the water column so that the deeper water, unaffected by turbulent heat exchange at the interface, rose from freezing to 1°C over a 12-hour period beginning at day 67.75. This approximates the ship's surface temperature record as shown in Fig. 12 of MKP. The ship drifted slightly ahead (downwind) of the ice band. The model was started from rest by imposing a wind stress that ramped linearly over 12 hours from zero to its value at day 66.5 in order to avoid inertial

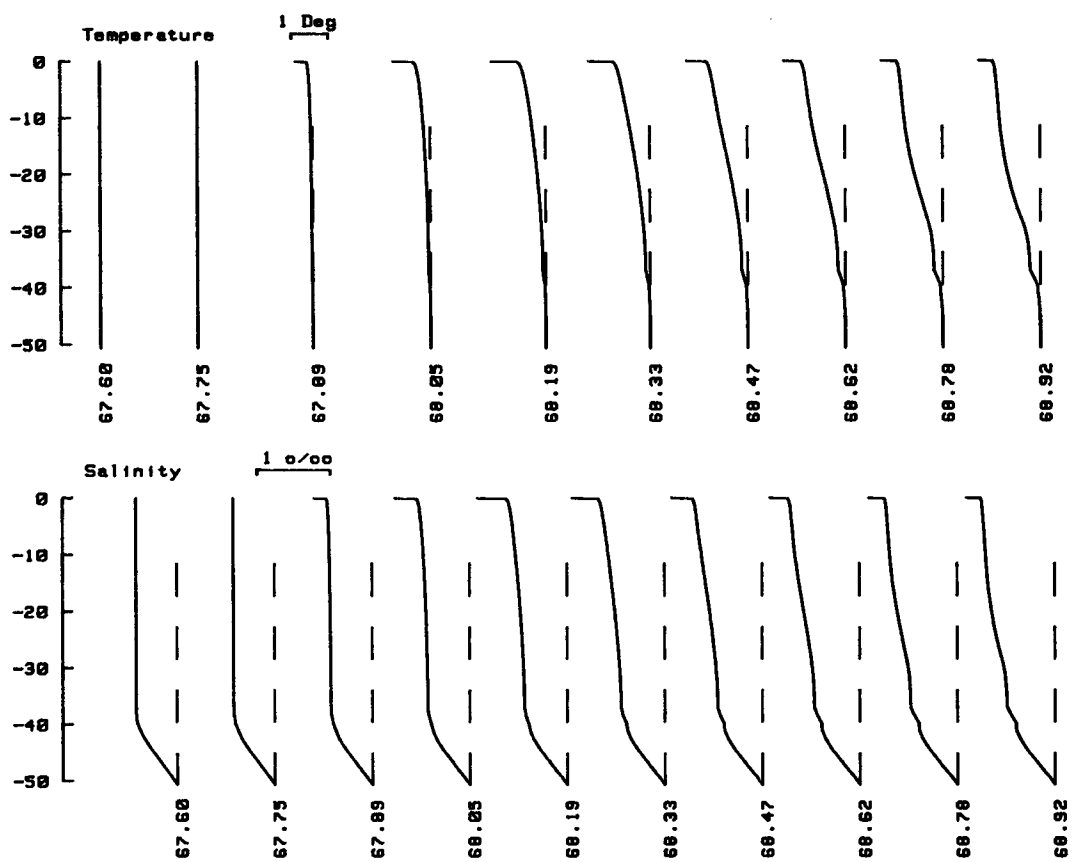

FIG. 15. Model (M2) temperature and salinity profiles every ¼ inertial period from 67.60 to 68.92. Note that temperature at 50 m increases from initial mixed-layer freezing point at 67.75 to 1°C at 68.25. Salinity at 50 m remains unchanged. Numbers beneath each profile indicate time in Julian days of 1981.

oscillations caused by impulsive forcing. The model was run with 15-min timesteps to day 69.0.

Surface velocity output was smoothed to remove inertial oscillation using an algorithm similar to that used to remove tidal motion from the position data, but modified to work directly on the velocity time series. Integrated displacement of the smoothed velocity for the period from 67.25 to 68.5 is shown for two model runs in Fig. 13, with the same format as Fig. 12. M1 refers to the model with constant z_0, M2 is the case where z_0 decreases over the heating period as described above, and W, fd, and I are as previously noted. Note the increase in both magnitude and deflection angle for each of the model runs. The surface velocity comparison over time is shown in Fig. 14 for M2.

Figure 15 shows model (M2) temperature and salinity profiles every one-quarter inertial period from just before the heating event to the end of the calculation. Recall that the temperature in the pycnocline rises from freezing to 1°C in the time period 67.75 to 68.25. As melting ensues, the upper ocean freshens and cools and a weak pycnocline is formed between 20 and 30 m depth.

Figure 16 shows model velocity profiles. Over the course of the numerical experiment the wind was relatively steady (see Fig. 16 of MKS), so the change in velocity structure results from the introduction of surface buoyancy. Of course, the observed ice divergence is only one facet of this pattern. It is likely that the complicated pattern of depth-dependent divergence implicit in these profiles would introduce important vertical velocities and local pressure gradients. The next step is to add at least another spatial dimension to the model, and we are progressing in that direction.

5. Conclusions

A model has been created that can describe the evolution of the vertical structure of the ocean surface layer under a melting or freezing ice layer. Interfacial boundary conditions are developed that are consistent with conventional near-surface, turbulent boundary layer methodology. In this paper the boundary conditions are used in conjunction with a second-moment turbulence closure model that provides vertical mixing coefficients along with turbulence kinetic energy. Solutions applicable to unsteady, horizontally homogeneous, melting or freezing problems can also be transformed—to good approximation—to steady, horizontally inhomogeneous problems.

In the case where ice melts due to underlying warm water, the problem is intrinsically unsteady and importantly governed by the stabilizing effect of the surface flux of fresh water. Thus, if ice impulsively overlays warm water, the melt rate is initially large—and de-

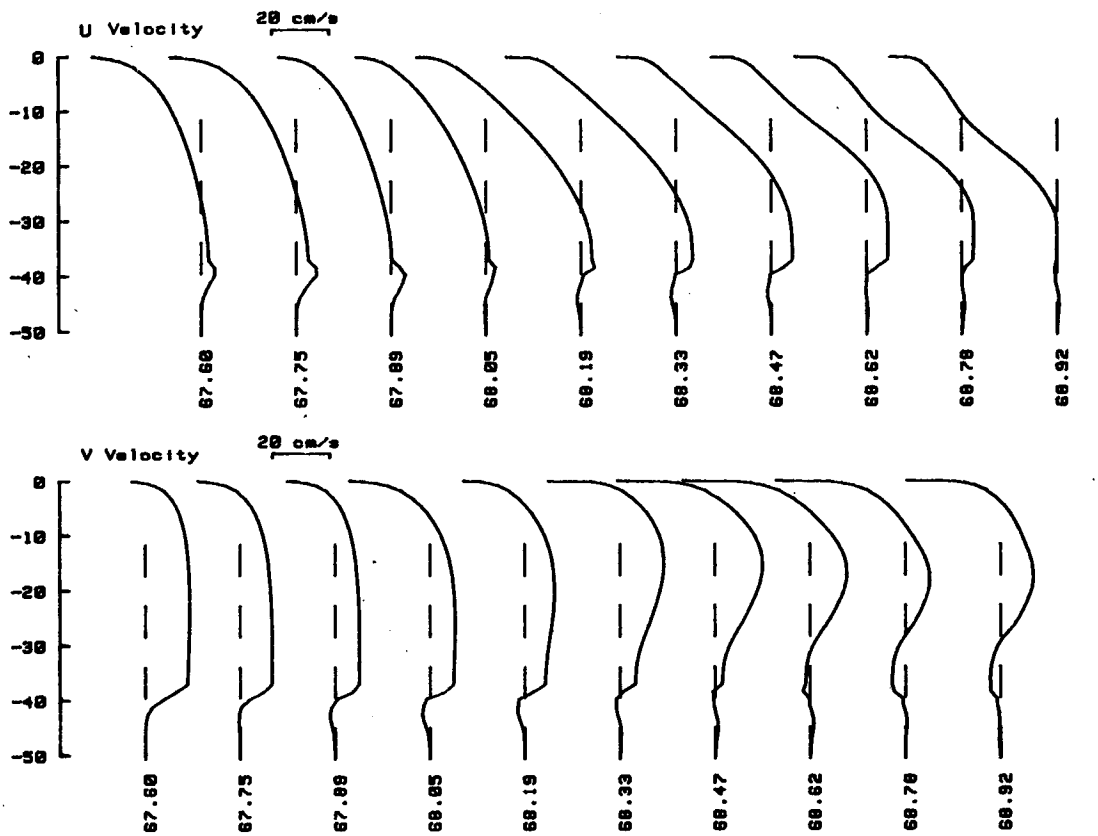

FIG. 16. As in Fig. 16, but eastward (U) and northward (V) velocity profiles are plotted.

pendent on the initial conditions and ice velocity or interfacial stress—but subsequently decreases as the surface-layer storage of thermal energy is depleted. Stabilization also reduces the interfacial drag coefficient and this appears to account for the observed divergence of ice packs in the marginal ice zone.

Other than the specific cases reported in this paper, the model has been run for multi-month periods and with transition from melting to freezing with no apparent problems. The model as described in this paper is suitable for insertion into two- and three-dimensional numerical models.

APPENDIX A

Effect of Vertical Advection

As an example we consider the temperature variable, the full equation for which is

$$\frac{\partial T}{\partial t}+U\frac{\partial T}{\partial x}+V\frac{\partial T}{\partial y}+W\frac{\partial T}{\partial z}=\frac{\partial}{\partial z}\left(K_H\frac{\partial T}{\partial z}\right). \quad \text{(A1)}$$

For small z, $W \approx$ constant $= W_0$. Then (A1) can be integrated to yield

$$(\alpha_t+K_H)\frac{\partial T}{\partial z}-W_0(T-T_0)=F_t+O(z). \quad \text{(A2)}$$

The $O(z)$ term is negligible in the law of the wall region and will hereafter be neglected.

Near the surface $K_H = ku_\tau z$. For large enough z, where $K_H \gg \alpha_t$, an integral of (A2) is

$$T-T_0=-\frac{F_t}{W_0}\left[1-\exp\left(\frac{W_0\xi}{ku_\tau}\right)\right] \quad \text{(A3)}$$

where we here define $\xi = \ln(z/z_0)$. If $W_0/u_\tau = O(1)$, then (A3) provides an important modification to the conventional law of the wall. However, for small W_0/u_τ, as is the case in this paper, the conventional law of the wall is recovered. Thus, while W_0 plays an important role in the interfacial energy and salinity balance, it can be neglected in the advection terms.

APPENDIX B

Extension of the Model to Include Frazil Ice Formation

To account for the creation of frazil ice requires modification of (2) and (3) such that

$$\frac{\partial T}{\partial t}=\frac{\partial}{\partial z}\left[(K_H+\alpha_t)\frac{\partial T}{\partial z}\right]+\sigma_i L \quad \text{(B1)}$$

$$\frac{\partial S}{\partial t}=\frac{\partial}{\partial z}\left[(K_H+\alpha_s)\frac{\partial S}{\partial z}\right]+\sigma_i(S-S_i) \quad \text{(B2)}$$

where σ_i is the volumetric fractional rate of ice creation. In addition, an ice concentration equation can be written according to

$$\frac{\partial C}{\partial t}+\frac{\partial}{\partial z}(W_dC)=\frac{\partial}{\partial z}\left[K_H+\frac{\partial C}{\partial z}\right]+\sigma_i \quad \text{(B3)}$$

where C is the (nondimensional) volumetric ice fraction and W_d is the drift velocity of the ice particles relative to the mean fluid velocity. An appropriate expression for the source term, σ_i, is

$$\sigma_i=\frac{1}{\tau}\frac{(mS-T)H(mS-T)}{L} \quad \text{(B4)}$$

where $H(mS-T)$ is the Heaviside function so that $\sigma_i = 0$ when $mS > T$. In Eq. B4 τ has dimensions of time and is related to the heat transfer rate between seawater and the ice particles; specifically, $\tau = [3.0\alpha_t \, \mathrm{Nu}C/(R_p^2)]^{-1}$ where Nu is the Nusselt number and R_p is the radius of the ice particles. For spherical particles at low Péclet number, Nu = 1. Similarly, W_d can be related to Stokes drag at low Reynolds number. At higher Reynolds numbers there is considerable uncertainty in the choice of τ and W_d.

Omstedt and Svenson (1984) have solved equations very similar but somewhat less general than the above using a different closure model. They did not include an ice–sea interface, and the total flux [turbulent flux plus gravitational drift flux, $(W_dC)_{z=0-}$] was effectively null (Svenson, personal communication, 1985). The paper, however, implies that only the turbulent flux was effectively null. Thus, on cooling, the ice concentration increased only near the surface (within the top 2 to 3 m) with the maximum concentration at the surface. The calculations were terminated when the surface concentration reached 5%; thereafter, flocculation would presumably occur and this would be followed by formation of an ice cover. Thus it would appear that their model represents the early stages of the freezing process. If one finds that this early stage is important then the present model can be enhanced (and made more complicated) by replacing (2) and (3) by (B1) and (B2) and adding (B3). The surface boundary conditions would have to be modified.

REFERENCES

Clarke, D. B., and S. F. Ackley, 1984: Sea ice structure and biological activity in the Antarctic marginal ice zone. *J. Geophys. Res.*, **89**, 2087–2096.

Garret, J. R., and B. B. Hicks, 1973: Momentum, heat and water vapour transfer to and from natural and artificial surfaces. *Quart. J. Roy. Meteor. Soc.*, **99**, 680–687.

Gow, A. J., S. F. Ackley, W. F. Weeks and J. W. Govani, 1982: Physical and structural characteristics of Antarctic sea ice. *Ann. Glaciol.*, **3**, 113–117.

Hibler, W. D., 1979: A dynamic thermodynamic sea ice model. *J. Phys. Oceanogr.*, **9**, 815–846.

——, and K. Bryan, 1984: Ocean circulation: its effect of seasonal sea-ice simulations. *Science*, **224**, 489–492.

Josberger, E. G., 1983: Sea ice melting in the marginal ice zone. *J. Geophys. Res.*, **88**, 2841–2844.

Kolmogorov, A. N., 1941: The local structure of turbulence in incompressible viscous fluid for very large Reynolds number. (in Russian). *Dokl. Akad. Nauk SSSR*, **30**, 299–303. [English translation, S. K. Topper, 1961: *Turbulence*, Interscience, 187 pp.]

Lewis, E. L., and R. G. Perkins, 1983: Supercooling and energy exchange near the Arctic Ocean surface. *J. Geophys. Res.*, **88,** 7681–7685.

Martin, S., P. Kauffman and C. Parkinson, 1983: The movement and decay of ice edge bands in the winter Bering Sea. *J. Geophys. Res.*, **88,** 2803–2812.

McPhee, M. G., 1981: An analytic similarity theory for the planetary boundary layer stabilized by surface buoyancy. *Bound.-Layer Meteor.*, **21,** 325–340.

——, 1982: Sea ice drag laws and simple boundary layer concepts, including application to rapid melting, Rep. 82-4, U.S. Army CRREL, Hanover, 17 pp.

——, 1983: Turbulent heat and momentum transfer in the oceanic boundary layer under melting pack ice. *J. Geophys. Res.*, **88,** 2827–2835.

——, 1984: Drift velocity during the drift station phase of MIZEX 83. MIZEX Bull. No. 4, 1–12.

Mellor, G. L., 1972: The large Reynolds number asymptotic theory of turbulent boundary layers. *Int. J. Eng. Sci.*, **10,** 852–873.

——, 1973: Analytic prediction of the properties of stratified planetary surface layers. *J. Atmos. Sci.*, **30,** 1061–1069.

——, and T. Yamada, 1974: A Hierarchy of turbulence closure models for planetary boundary layers. *J. Atmos. Sci.*, **31,** 1791–1806. [Corrigendum, 1977: *J. Atmos. Sci.*, **34,** 1482.]

——, and ——, 1982: Development of a turbulence closure for geophysical fluid problems. *Rev. Geophys. Space Phys.*, **20,** 851–875.

Omstedt A., and U. Svenson, 1984: Modeling supercooling and ice formation in a turbulent Ekman layer. *J. Geophys. Res.*, **89,** 735–744.

Rotta, J. C., 1951a: Statistiche theorie nichthomogener turbulence, 1. *Z. Phys.*, **129,** 547–572.

——, 1951b: Statistiche theorie nichthomogener turbulence, 2. *Z. Phys.*, **131,** 51–77.

Schlicting, H., 1975: *Boundary Layer Theory,* McGraw-Hill, 646 pp.

Sverdrup, H. U., 1951: Evaporation from the oceans. *Compendium of Meteorology,* T. F. Malone, Ed., Amer. Meteor. Soc., 1071–1081.

Sheppard, P. A., 1958: Transfer across the Earth's surface and through the air above. *Quart. J. Roy Meteor. Soc.*, **84,** 205–224.

Wadhams, P., 1983: A mechanism for the formation of ice edge bands. *J. Geophys. Res.*, 2813–2818.

Weeks, W. F., and S. F. Ackley, 1982: *The growth, structure and properties of sea ice. CRREL Monogr.* 81-1, U.S. Army CRREL, Hanover, 1–130.